

Influence of interface dipole layers on the performance of graphene field effect transistors

Naoka Nagamura^{1,2}, Hirokazu Fukidome^{3,}, Kosuke Nagashio⁴, Koji Horiba⁵, Takayuki Ide³, Kazutoshi Funakubo³, Keiichiro Tashima³, Akira Toriumi⁴, Maki Suemitsu³, Karsten Horn⁶, and Masaharu Oshima⁷*

¹National Institute for Materials Science, 1-2-1 Sengen, Tsukuba, Ibaraki 305-0047, Japan

²PRESTO, Japan Science and Technology Agency, 4-1-8 Honcho, Kawaguchi, Saitama 332-0012, Japan

³Research Institute of Electrical Communication, Tohoku University, 2-1-1 Katahira, Aoba-ku, Sendai 980-8577, Japan

⁴Department of Materials Engineering, Graduate School of Engineering, The University of Tokyo, 7-3-1 Hongo, Bunkyo-ku, Tokyo 113-8656, Japan

⁵Photon Factory, Institute of Materials Structure Science, High Energy Accelerator Research Organization, 1-1 Oho, Tsukuba, Ibaraki 305-0801, Japan

⁶Department of Physical Chemistry, Fritz Haber Institute of the Max Plank Society, 14195 Berlin, Germany

⁷Synchrotron Radiation Research Organization, The University of Tokyo, 7-3-1 Hongo, Bunkyo-ku, Tokyo 113-8656, Japan

*Corresponding authors

Email: fukidome@riec.tohoku.ac.jp; Tel: +81-22-217-5484 (Hirokazu Fukidome)

Abstract

The linear band dispersion of graphene's bands near the Fermi level gives rise to its unique electronic properties, such as a giant carrier mobility, and this has triggered extensive research in applications, such as graphene field-effect transistors (GFETs). However, GFETs generally exhibit a device performance much inferior compared to the expected one. This has been attributed to a strong dependence of the electronic properties of graphene on the surrounding interfaces. Here we study the interface between a graphene channel and SiO₂, and by means of photoelectron spectromicroscopy achieve a detailed determination of the course of band alignment at the interface. Our results show that the electronic properties of graphene are modulated by a hydrophilic SiO₂ surface, but not by a hydrophobic one. By combining photoelectron spectromicroscopy with GFET transport property characterization, we demonstrate that the presence of electrical dipoles in the interface, which reflects the SiO₂ surface electrochemistry, determines the GFET device performance. A hysteresis in the resistance vs. gate voltage as a function of polarity is ascribed to a reversal of the dipole layer by the gate voltage. These data pave the way for GFET device optimization.

1. Introduction

Interfaces of a graphene channel, such as those with gate oxides or contact metals, demand precise and accurate control of electronic level alignment. In graphene, the linear band dispersion near the Fermi level in principle provides excellent intrinsic electronic properties, e.g. an extremely high mobility of carriers, derived from their zero-effective mass. These intrinsic properties make graphene a

promising material for next-generation electronics applications, such as graphene-based field-effect transistors (GFETs) and high-electron mobility transistors (HEMTs). At present, however, actual graphene channels used in GFETs actually exhibit transport properties inferior to those anticipated from the intrinsic electronic properties¹⁻⁴. This inferiority is ascribed to the high susceptibility of the electronic properties of graphene to the surrounding interfaces as well as to technological immaturity in graphene device fabrication. This high susceptibility is also in part due to the linear band dispersion. In conventional semiconductors, the average kinetic energy per electron is $E_K \sim \hbar^2 n_d^{2/d} / 2m^*$ where m^* is the effective mass and n_d is the average electron density in d spatial dimensions. The Coulomb energy per electron is of the order $E_C \sim e^2 n_d^{1/d} / \epsilon_0$ where e is the electron charge. Therefore, the effective coupling constant α_{eff} , which indicates the ratio of Coulomb over kinetic energy and is related to the strength of the electron-electron interactions, is given by $\alpha_{\text{eff}} = E_C / E_K = 2m^* e^2 n_d^{-1/d} / \hbar^2 \epsilon_0$. This depends on carrier density. On the other hand, the average kinetic energy per electron in graphene is of the order $E_K \sim \hbar v_F n^{1/2}$ where v_F is the Fermi-Dirac velocity and n is the 2D electronic density, owing to its linear dispersion. So, the α_{eff} in 2D graphene is described as $\alpha_{\text{eff}} = E_C / E_K = (e^2 / \epsilon_0) / \hbar v_F$. This is independent of the electronic density, but affected by the dielectric constant of the surrounding environment⁵⁻⁷.

Of the various interfaces, the interface with gate oxides is of particular concern^{8,9} because oxide films are the most popular materials for insulating layers in semiconductor devices. The interface between a graphene channel and a gate oxide not only acts as scattering centers for carriers but also causes drastic changes

in electronic characteristics of graphene such as e-e interactions described above. Changes in the dielectric constants of gate oxides, such as SiO₂, thus influence the transport properties or in other words, the device performance¹⁰; for example, depositing ice on a graphene channel enhances carrier mobility in the channel¹¹. This is explained by a reduction in α_{eff} by the high dielectric constant of ice. Hence the interface chemistry also influences the transport properties. This is shown by reports that a graphene channel interfaced with hydrophilic SiO₂ exhibits degraded transport properties, such as a reduced carrier mobility and hysteresis in the resistance-gate bias curve in the gate-bias sweep direction, when compared to a channel interfaced with hydrophobic SiO₂^{12,13}. The difference between hydrophobic and hydrophilic SiO₂ lies in the presence of adsorbed water molecules on the latter, which are sandwiched between graphene and hydrophilic SiO₂¹⁴.

The impact of interface physics and chemistry on graphene channels should thus be fully understood for further development in the GFET technology. Imaging techniques are most useful to extract interface characteristics and microstructures¹⁵⁻¹⁸. To this end, we have developed a core-level photoelectron spectromicroscopy technology, called “3D nano-ESCA,” where we can scan the sample with a high lateral spatial resolution (70 nm)¹⁹ to record photoelectron spectra (the “third dimension”) to quantitatively analyze electronic level information, such as the Fermi level in graphene, and also chemical states, for example the oxidation valency of SiO₂ at the desired points, from core level line positions²⁰. We have demonstrated in our previous reports that 3D nano-ESCA is useful for the microscopic investigation of GFETs^{21,22}. In fact, microscopic spatial variations of the potential landscape in a GFET were elucidated by measuring the

Fermi level using 3D nano-ESCA. Thus, 3D nano-ESCA is a most suitable tool to analyze electronic states, chemical states and, indirectly, transport properties.

This study describes how SiO₂ surface chemistry, i.e., hydrophilicity vs. hydrophobicity, modulates the electronic states of the graphene channel from a microscopic viewpoint and then compares the influence of states with the transport properties obtained from the macroscopic electrical characteristics of GFETs.

2. Methods

2.1. Sample Preparation

Exfoliated graphene was transferred onto SiO₂ thin films (90 nm) on p⁺-Si(100) substrates. The color contrasts in optical images depending on the layer number were emphasized at the graphene sheets on 90 nm SiO₂/Si substrates, so the presence of a mono-layer of graphene was confirmed by the optical contrasts and Raman spectroscopy²³. To prepare a hydrophobic SiO₂ thin film, we performed the so-called reoxidation process of the SiO₂ thin film by annealing it at 1273 K for 5 min in a 100% oxygen gas flow¹³. This process induces the desorption of H₂O molecules from the surface and produces surface siloxane groups. On the other hand, to prepare hydrophilic SiO₂ thin films, an O₂ plasma treatment with an O₂/Ar mixture (1:9) flow rate of 50 cm³/min was carried out¹³. After the exfoliation of monolayer graphene on the prepared SiO₂ thin films, Ni contact electrodes were prepared by vacuum evaporation, and structured by electron-beam lithography. The post annealing procedure was not adopted, and the measurements for sample characterization were performed on as-fabricated devices.

2.2. Sample Characterization

Spatially resolved C $1s$, Si $2p$, and O $1s$ core-level photoelectron spectra measurement was carried out using the 3D nano-ESCA instrument installed at the University of Tokyo outstation beamline, BL07LSU at SPring-8^{19,24}. In this beamline, the synchrotron radiation (SR) beam has a high energy-resolving power ($E/\Delta E > 10^4$). The photon energy of the SR beam used for measurements was 1000 eV. The lateral spatial resolution, i.e., the spot size of the X-rays focused using a Fresnel zone plate, was 70 nm. The energy resolution of the spectrometer was set to 300 meV and the accuracy of the angle resolution was 0.9° . The binding energy scale was calibrated using the photoelectron peaks of a gold mesh foil (Au $4f_{7/2}$, binding energy: 84.0 eV) at the same potential as the source electrode, and the Fermi levels detected in valence spectra on Ni electrodes. Details of the experimental setup can be found elsewhere^{19,22}. The resistance-gate voltage characteristics were evaluated in ambient air conditions using a semiconductor parameter analyzer (B1500A, Keysight Technologies Inc.).

3. Results and Discussion

To quantitatively analyze the impact of SiO₂ surface chemistry on band level alignment, we first demonstrate the applicability of 3D nano-ESCA; we then discuss the influence of interface chemistry between graphene and SiO₂ on the channel performance. In section 3.3, we compare the electronic states with the device performance (e.g., hysteresis), which varies with SiO₂ surface chemistry, and finally in section 3.4, we show that SiO₂ surface chemistry affects the electronic states of graphene near metal contacts as well.

3.1. 3D nano-ESCA Imaging of GFET

3D nano-ESCA, as illustrated in Fig. 1(a), is used to analyze the electronic structure of a GFET and to quantitatively clarify the effect of surface chemistry of SiO₂ thin films on the graphene channel. A GFET structure on a 1 cm × 1 cm substrate is mounted on a sample holder as shown in Fig. 1(b). Electrodes, including source, drain, and gate, are connected to the chamber ground. The optical micrograph of the GFET device structure consisting of a graphene flake channel region and contact metal electrodes is shown in the upper picture in Fig. 1(c). The faint shape of the graphene flake is barely visible. On the other hand, highly spatially resolved elemental mapping of the GFET device, where the intensities of the C 1s, Si 2p, and Ni 3p core-level spectra are red, green, and pink, respectively, are shown in the lower picture of Fig. 1(c), which is the same region as the upper one. A sharp image is obtained by using the nano-focused X-ray beam (70 nm) with a Fresnel zone plate¹⁹. 3D nano-ESCA thus has a high enough lateral spatial resolution to reflect the GFET architecture. As discussed above, hydrophobic SiO₂ thin films deposited on Si(100) substrates were subjected to the so-called reoxidation process, which leads to the surface being covered by siloxane groups (Fig. 1(d)), while the hydrophilic one is covered with silanol groups (Fig. 1(e))^{13,22}. The cross sections of both devices are schematically shown in Figs. 1(d) and 1(e), respectively.

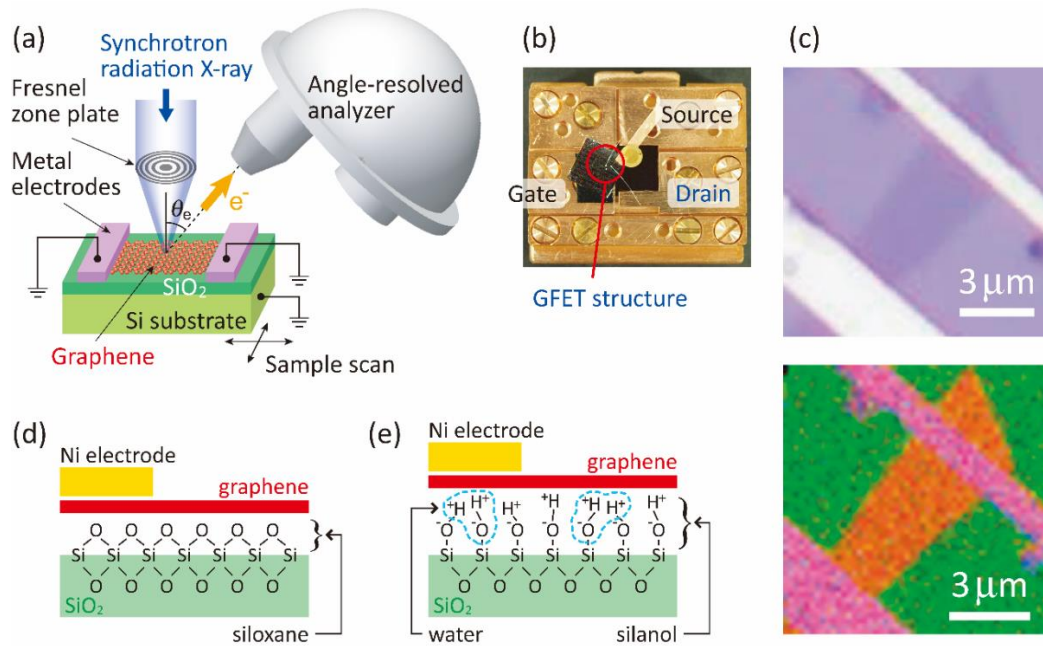


Figure 1 | Schematic of the measurements and graphene-oxide interface in GFET. (a) Schematics of the 3D nano-ESCA imaging system. (b) Photo of a sample holder upon which a GFET device structure on a substrate is mounted. (c) (upper) Optical micrograph of a GFET, barely showing the graphene flake. (lower) Elemental mapping of a GFET using 3D nano-ESCA, where green is the silicon substrate, pink are the nickel contacts, and red the graphene flake. (d, e) Schematic cross-sections of Ni electrodes and graphene on (d) hydrophobic and (e) hydrophilic SiO₂ thin films, respectively, indicative of the chemical composition.

3.2. Interface Chemistry of Graphene with SiO₂

The electronic and chemical states at the interfaces of graphene channels in GFETs with hydrophobic or hydrophilic SiO₂ films were examined by performing a point-for-point spectroscopic analysis of the C 1s, Si 2p, and O 1s core levels at the center of the graphene channels with 3D nano-ESCA, as shown in Figs. 2 and 3.

Along the graphene channels, we used the core-level binding energies to investigate the potential level alignment of graphene on the hydrophobic (blue curves in Figs. 2 and 3) and hydrophilic (red curves in Figs. 2 and 3) SiO₂ thin films on the Si(100) substrates. The C 1s spectrum of graphene on the hydrophobic SiO₂ thin film on Si(100) has a higher binding energy, compared to that on the hydrophilic SiO₂ thin film on Si(100) (Fig. 2(a)). The C 1s spectra can be decomposed into two components by precisely examining the binding energy, which directly reflects the Fermi level position relative to the Dirac point, of the graphene channels (Fig. 2(b)). The lower binding energy component is attributed to graphene, while the higher binding energy component, which is somewhat broader, is attributed to contaminations probably arising from lithographic processing, according to our previous angle-resolved analysis of the C 1s spectra of GFETs²². Although these contaminants could have an influence as p-type dopants and scattering centers in the graphene channels²⁵, the amount of residual carbon contaminants is almost the same between graphene channels on hydrophilic SiO₂ and hydrophobic SiO₂ according to the intensity of peak components assigned to contaminants in Fig. 2(b), so we assume that the effect of contaminants is the same on the hydrophilic and hydrophobic SiO₂. It is obvious that the peak of graphene on a hydrophilic SiO₂ thin film has a lower binding energy than that on a hydrophobic SiO₂ thin film. This result can be explained by the fact that doping induces a shift in the Fermi level, resulting in a shift in the C 1s binding energy²⁶, as schematically shown in Fig. 2(c). The binding energy of graphene on a hydrophobic SiO₂ thin film is 284.45 eV, which is very close to that of neutral graphene^{27,28}. Graphene on a hydrophobic SiO₂ thin film on Si(100) therefore exhibits negligible doping; on the other hand, it

can be inferred from the lower binding energy (284.23 eV) of the C 1s peak that graphene on a hydrophilic SiO₂ thin film is hole-doped. The difference between the spectra is about 0.22 eV. Assuming a linear band dispersion of graphene with respect to the wave vector, we use the following equation to estimate the concentration of doped holes (N_h) as follows^{29,30},

$$E_{DP} - E_F = \hbar v_F \sqrt{\pi} \sqrt{N_h} \quad (1)$$

Here, E_F , E_{DP} , \hbar , and v_F are the Fermi level, Dirac point energy, reduced Planck's constant, and the Fermi velocity of electrons in graphene ($\sim 1.1 \times 10^6$ m/s), respectively. Inserting our experimental value of 0.22 eV as the value of $(E_{DP} - E_F)$, the concentration of the doped holes (N_h) in graphene on hydrophilic SiO₂ thin films is estimated to be 2.4×10^{12} cm⁻². The SiO₂ surface chemistry thus has a strong influence on the Fermi level position relative to the Dirac point, i.e., the doping strength, in the graphene channel.

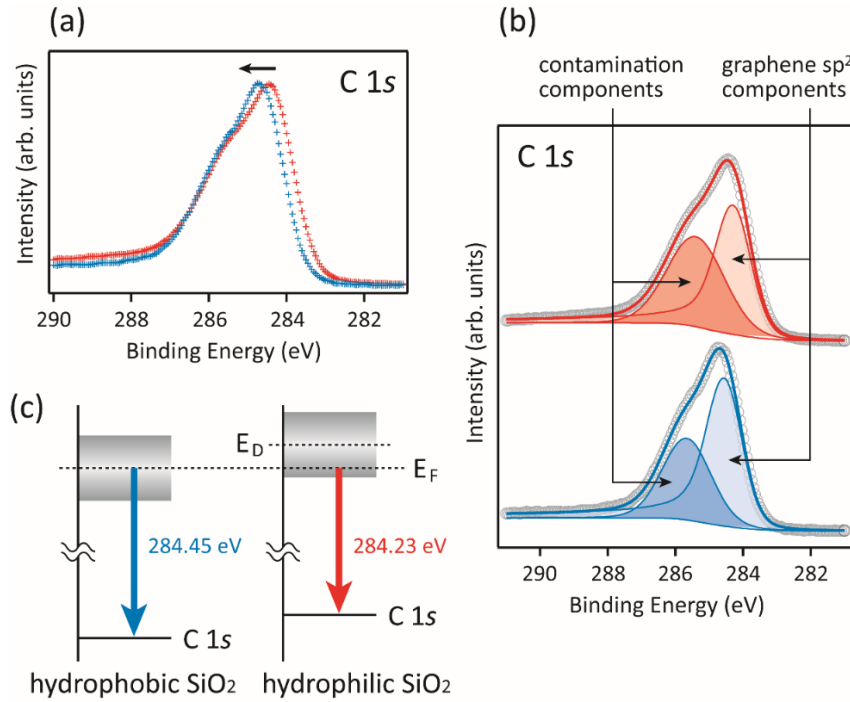


Figure 2 | Electronic states of graphene channels in contact with SiO₂ gate

oxides. (a) Pinpoint C 1s core-level spectra recorded at the center of the graphene channels on hydrophobic (blue) and hydrophilic (red) SiO₂ thin films on Si(100) substrates. (b) Decomposition of the spectra displayed in (a). (c) Schematic diagram to explain the peak shift in graphene at different SiO₂ surface conditions. For comparison, the data on hydrophilic SiO₂ thin films was sourced from²².

In order to investigate the influence of SiO₂ surface chemistry on the electronic states of graphene, pinpoint measurements of the Si 2p and O 1s core lines of the SiO₂ thin films underneath graphene were conducted at the center of the graphene channels, as shown in Figs. 3(a) and (b), respectively, with the decomposition of these core lines shown in Figs. 3(c) and (d). The Si 2p core lines of hydrophobic SiO₂ contain a small shoulder around 103 eV, which is not observed in hydrophilic SiO₂. This shoulder, which occurs at lower binding energies, is ascribed to the surface siloxane, as schematically shown in Fig. 1, which has a lower valency than stoichiometric SiO₂³¹. This is corroborated by the angle dependence of the peak intensity ratio of the siloxane peak over the bulk SiO₂ peak (Figs. 4(a) and (b)); the results indicate that siloxane is present on the surface. Both the O 1s and Si 2p core lines of the hydrophilic SiO₂ thin film are shifted towards lower binding energies by a considerable amount (~1.2 eV) when compared to the shifts in their counterparts corresponding to the hydrophobic SiO₂ thin film. This means that there is an interfacial layer that affects the binding energies.

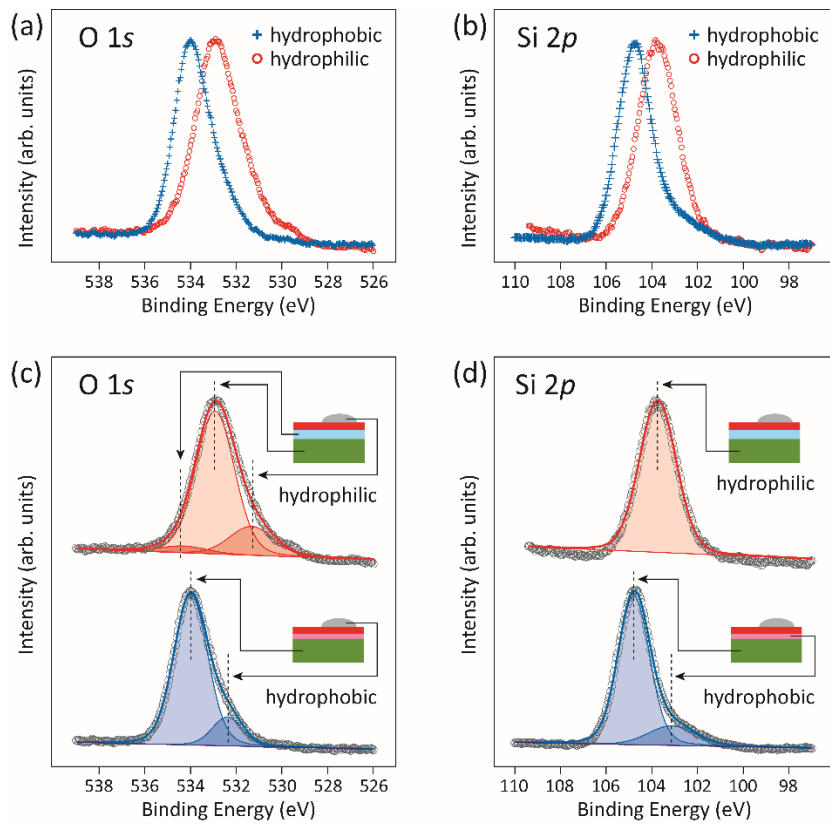


Figure 3 | Electronic and chemical states of the SiO₂-graphene channel interface. (a, b) Si 2*p* and O 1*s* core level spectra at the center of the graphene channels on hydrophobic (blue plus sign) and hydrophilic (red circle) SiO₂ thin films on Si(100) substrates, respectively. For comparison, the data of a hydrophilic SiO₂ thin films is sourced from ref. 22. **(c, d)** Decomposed Si 2*p* and O 1*s* spectra, respectively.

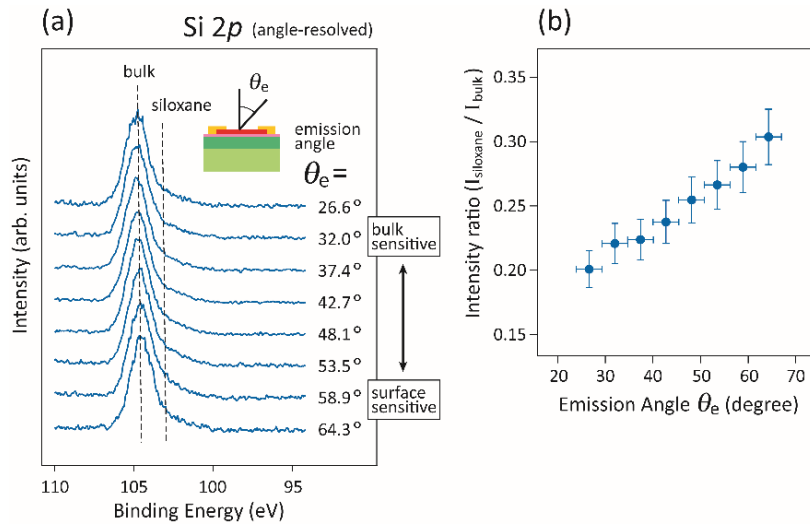


Figure 4 | Emission angle dependence of surface siloxane and bulk SiO₂.

(a) Si 2p core level spectra measured in various emission angles. Photoelectron signal from grazing angle is surface sensitive, and that from near normal angle contains information of buried bulk regions. (b) Emission angle dependence of the intensity ratio between the shoulder peak at 103 eV derived from the surface siloxane and the main peak component at 105 eV derived from the bulk SiO₂ substrate.

We interpret the shift towards lower binding energies as being not of chemical origin, they would be too large anyway, but due to the potential alignment in the GFET device. The difference in binding energies is very similar (the width of the O 1s peak is slightly different and there is a chemical shift which reveals itself by the presence of a second component in both interfaces). The considerable shift in binding energies can be analyzed using the schematic band diagram of graphene/SiO₂/Si interfaces in GFETs (Fig. 5(a)). In our pinpoint analysis, the graphene channel, metal contacts, and back gate (Si substrate) are grounded, i.e., the applied gate bias (V_G) = 0 V, as shown in Fig. 1(b). The Fermi level then

extends through all three materials as a straight line. Band alignment at the Si/SiO₂ interface can be derived from the Fermi level at the Si surface²⁰. SiO₂, which has a large bandgap (~ 9 eV), causes a large potential drop in the Si substrate at the interface, as shown in Fig. 5(a).

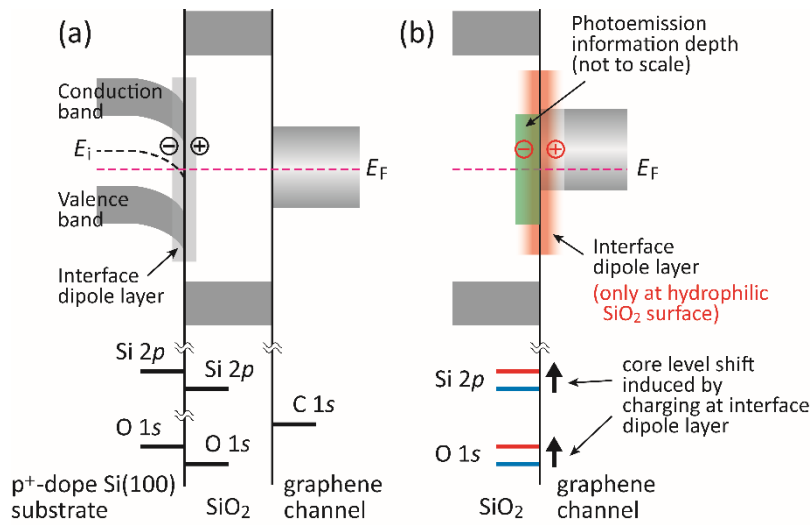


Figure 5 | Schematic band diagrams of interfaces in GFET structures. (a) Schematic band diagram across the GFET. **(b)** Schematic band diagram of graphene and SiO₂ thin films to demonstrate the influence of SiO₂ surface chemistry.

A comparison of graphene/hydrophobic SiO₂ and graphene/hydrophilic SiO₂ interfaces, in terms of the binding energies of the core levels and valence band, is shown in Fig. 5(b). Here, the Fermi level of SiO₂ is again aligned with that of graphene. We could detect the graphene, the topmost layer of the SiO₂ thin film under graphene, and the graphene/SiO₂ interface because the probing depth was a few nanometers, considering the escape depth of photoelectrons with a kinetic energy of about 500 (O 1s) and 900 (Si 2p) eV³² at the incident photon energy 1000

eV. The binding energies of the Si $2p$ and O $1s$ core levels thus reflect the changes in valence band alignment with respect to the Fermi level. The point to be noted is the presence or absence of a dipole layer at the graphene/SiO₂ interface, which depends on the SiO₂ surface chemistry. With respect to the graphene/hydrophilic SiO₂ interface, graphene and SiO₂ are charged positively and negatively, respectively, as can be inferred from the shifts in the C $1s$ (Fig. 2(a)), Si $2p$ (Fig. 3(a)), and O $1s$ core levels (Fig. 3(b)). We attribute the existence of silanol groups on the surface of the hydrophilic SiO₂ thin film to the negative charges on the surface. According to previous theoretical predictions, neither silanol nor siloxane groups cause doping in graphene³³. While this prediction awaits experimental confirmation, the potential shift due to silanol groups, when in contact with water molecules, may be causing the doping in graphene. In fact, this suggestion is supported by the low value of the acid-dissociation constant (pK_a) of the SiO₂ surface (~ 4.5)³⁴, which indicates a negative charge by the process of giving up a proton in water, which has a higher value pK_a (pH) of 7. This has been verified by in-situ electrochemical Fourier transform infrared spectroscopy (FTIR) in combination with quantum chemical calculations, which indicate that negatively charged silanol groups are formed when a SiO₂ surface is in contact with water³⁵. Furthermore, our suggestion is supported by previous theoretical studies pointing out the role of water in the doping of graphene on substrates such as SiO₂^{36,37}. The dipole layer thus consists of positively-charged graphene and a negatively-charged hydrophilic SiO₂ thin film, resulting in a potential drop in the layer, as shown in Fig. 5(b). The potential drop shifts the energy position of the Si $2p$ and O $1s$ core lines upwards relative to the Fermi level. In the case of the hydrophobic SiO₂ thin

film, no dipole layer is present at the interface, hence graphene is not doped, (see Fig. 2), when the surface of the hydrophobic SiO₂ thin film is covered with uncharged siloxane groups. A negligible dipole layer is then formed at the interface. This results in a negligible potential drop, as expressed by the straight line across the interface (Fig. 5(b)). Thus, pinpoint core level spectroscopy demonstrates that the SiO₂ surface chemistry has a great impact on the interfacial electronic level alignment between graphene and SiO₂.

3.3. Influence of SiO₂ Surface Chemistry on GFET Electrical Characteristics

The above difference in level alignment in graphene on a hydrophilic or hydrophobic SiO₂ substrate is expected to have a strong influence on GFET electrical characteristics as well^{12,13}, because the electronic states of the graphene channel determine the GFET electrical characteristics. Therefore, we compared the resistance (R)-gate voltage (V_G) curves of GFETs using hydrophobic and hydrophilic SiO₂ thin films as the gate oxides, as shown in Fig. 6(a). In the GFETs, Ni thin films and p⁺-Si(100) substrates are used as the source/drain electrodes and back gate, respectively. The most striking feature in these curves is the large hysteresis found in the R - V_G curve of the GFET using a hydrophilic SiO₂ thin film as the gate oxide, but not in the GFET using hydrophobic SiO₂^{12,13}. The curves for forward and backward sweep on hydrophobic SiO₂ are identical and are thus not resolved in Fig. 6(a). Such hysteresis, which is reproduced over many consecutive sweeps¹³, indicates that the doping type changes with a change in the direction of the gate voltage sweep. Because the dipole layer induces a difference in the level alignment between the two GFETs (Fig. 5(b)), it is obvious that the dipole layer

formed between graphene and the hydrophilic SiO₂ thin film affects the doping level of the graphene channel, as schematically shown in Fig. 6(b). What we observe here is that the reversal of gate voltage inverts the polarity of the dipole layer, which arises from the polarity inversion of the charging states of graphene and the hydrophilic SiO₂ surface. As an aside we note that the consumption of gate voltage by the dipole layer (Fig. 6(b)) can cause a broadening in the width of the R - V_G curve of the GFET with hydrophilic SiO₂ rather than hydrophobic SiO₂³⁸. This is because the effective gate capacitance C increases by the dipole layer in the formula³⁹ which represents the graphene resistance R ;

$$R = \frac{L}{w} \times \frac{1}{e\mu \sqrt{n_0^2 + (C|V_G - V_D|)^2}} + R_C, \quad (2)$$

where L/w is the aspect ratio of the transistor, μ is the mobility, n_0 is the residual charge, and R_C is the constant background resistance.

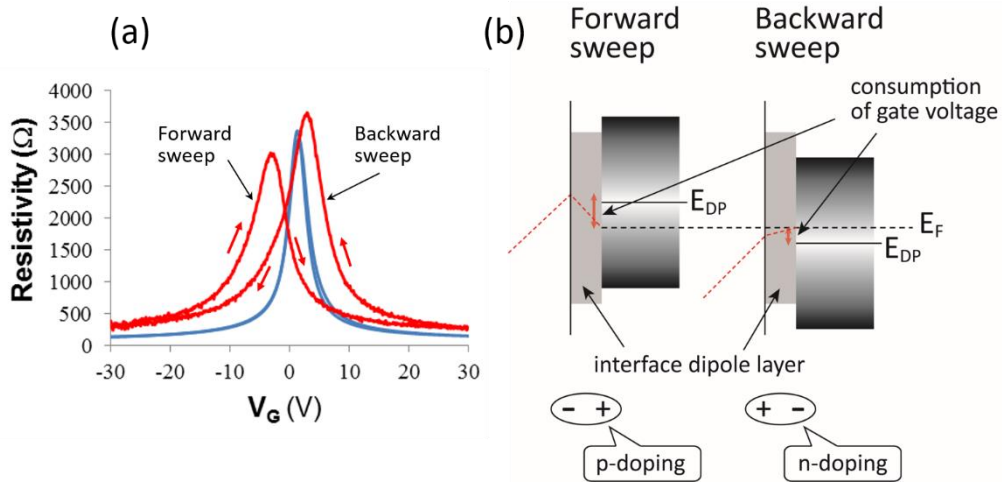


Figure 6 | Influence of SiO₂ surface chemistry on GFET electrical characteristics. (a) R - V_G curves of the GFETs using hydrophobic (blue) and hydrophilic (red) SiO₂ thin films on Si(100) substrates. (It should be explained

in the Figure which of the red curves is forward and backward) No hysteresis occurs in graphene on hydrophobic SiO₂, hence the forward and backward sweep coincide. **(b)** Schematic diagram explaining the mechanism behind the hysteresis of the R - V_G curve; the interface dipole layer plays a crucial role.

The next thing to be discussed is the comparison of Dirac voltages of the GFETs, where the resistivity (R) is the highest and the Fermi level is considered to coincide with the Dirac point, by relating the results obtained by 3D nano-ESCA, as described in the previous subsection. To relate with the 3D nano-ESCA measurements, we used the R - V_G curve in the forward sweep for the GFET using a hydrophilic SiO₂ thin film. The reason for this choice is as follows. The R - V_G curves were measured by sweeping V_G from -30 V to $+30$ V (forward sweep) and later from $+30$ V to -30 V (backward sweep); it was stopped at -30 V, after which 3D nano-ESCA measurements at $V_G = 0$ V were carried out. Therefore, these measurements can be regarded to occur during a forward sweep. The Dirac voltage of the GFET using a hydrophilic SiO₂ thin film in the forward sweep is more positive than that recorded using a hydrophobic SiO₂ thin film. This indicates the graphene channel in the GFET using a hydrophilic SiO₂ thin film in the forward sweep is more hole-doped than that using a hydrophobic SiO₂ thin film. This result is consistent with the pinpoint C 1s core level spectra of the graphene channel, which indicate the binding energy shift toward lower energy on a hydrophobic SiO₂ thin film due to hole doping as shown in Fig. 2, although we must consider adsorbed molecules other than water, such as O₂, during the R - V_G measurements^{12,14}. These changes in the R - V_G curves are thus explained by the

modulation in the electronic states of graphene channels in terms of their interface chemistry with SiO₂ gate oxides, which was described in the previous subsection as demonstrated through 3D nano-ESCA.

3.4. Influence of SiO₂ Surface Chemistry near the Metal Contact

Surprisingly, SiO₂ surface chemistry also exerts an influence on the electronic states near the interface with the metal contact, which is also a key component in GFET. One of the consequences of such metal-contact influence is the formation of a charge transfer region (CTR)^{13,40}, which can extend up to a width of 1 μm in the GFET using hydrophilic SiO₂ as the gate oxide²². The CTR is supposed to be formed due to the disappearance of the density of states (DOS) near the Dirac point in graphene. Unfortunately, however, the influence of SiO₂ surface chemistry on the CTR is still unclear.

To clarify the influence of SiO₂ surface chemistry on the electronic states of the graphene channel near the interface between graphene and contact metal, we performed spatially resolved C 1s core level spectroscopy near the metal contact using 3D nano-ESCA. The spatial variation in the binding energy of graphene, which reflects the change in doping (work function), on hydrophilic and hydrophobic SiO₂ thin films is shown in Fig. 7. It can be inferred that across the entire measured range, the binding energy of graphene on a hydrophilic SiO₂ thin film is smaller than that on a hydrophobic SiO₂ thin film. This means that graphene on a hydrophilic SiO₂ thin film is more positively charged, compared to that on a hydrophobic SiO₂ thin film. The value of binding energy (~ 284.45 eV), which is very close to that of neutral graphene²⁷, indicates that the graphene channel is negligibly doped when a

hydrophobic SiO₂ thin film was used, in agreement with the data in Figure 2.

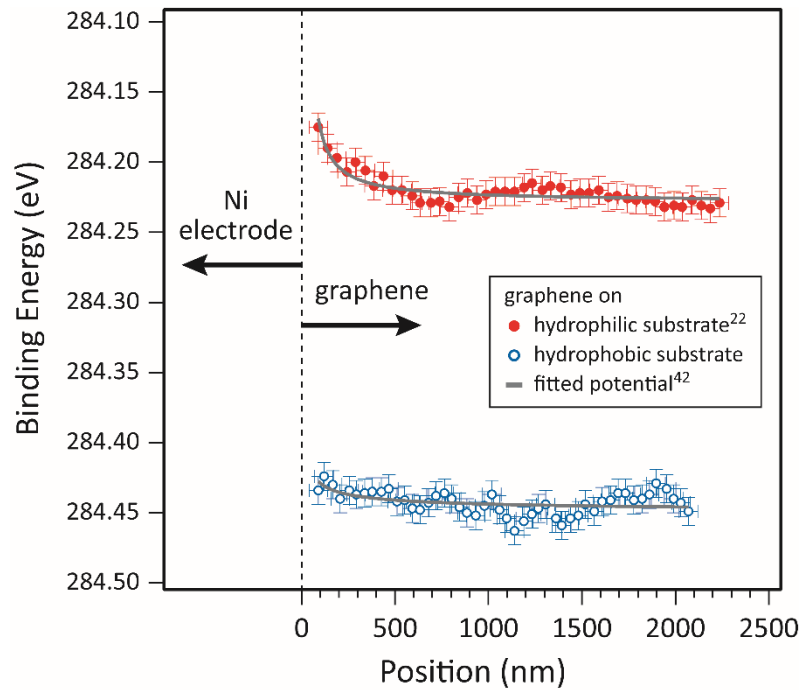


Figure 7 | Influence of SiO₂ surface chemistry on the potential variation across the graphene-contact metal interface. Change in the C1s core level of graphene peak across the graphene/Ni interface in GFETs using hydrophilic (red) and hydrophobic (blue) SiO₂ thin films as the gate oxides. For comparison, data on hydrophilic SiO₂ thin films is sourced from ref. 22.

In sharp contrast to the hydrophobic SiO₂ thin film, the binding energy of graphene on hydrophilic SiO₂ becomes smaller near the contact metal as shown in Fig. 7. The binding energy shift originates from local charge density as shown in Fig. 2(c), so the results which display the spatial distribution of the binding energy shift in Fig. 7 can be interpreted as a direct measurement of the screening potential in graphene. Sub-micron CTR formation is detected in the graphene channel on the

hydrophilic substrate, as reported in previous studies²². The determining factor in CTR formation is, in principle, supposed to be the charge transfer between materials of different work functions¹³, 4.5 eV for graphene and 5.4 eV for Ni⁴¹, which thermodynamically equilibrate the graphene/Ni system²².

To explain the difference in the screening potential of the hydrophilic and hydrophilic substrates, we performed theoretical estimations of the screening potential according to the Thomas-Fermi approach proposed by Khomyakov *et al.*⁴². For a single layer of graphene, they described the screening potential in terms of the charge density in an ungated condition as follows

$$V(x) = \mu_F + \text{sign}(\sigma) \sqrt{\left| \frac{V_B |V_B|}{x/l_s} - \mu_F |\mu_F| \right|} \quad (3)$$

where x is the distance from the metal/graphene contact edge, $l_s = \hbar v / \pi \alpha |V_B|$ is a scaling length, $V_B = V_{B1} + V_{B2}$, $\hbar v = 6.05 \text{ eV} \cdot \text{\AA}$, and $\alpha = e^2 / 4\pi \epsilon_0 \kappa \hbar v = 2.38 / \kappa$ is the fine-structure constant in graphene. κ is the effective dielectric constant. V_{B1} and V_{B2} are boundary potential constants, which can be written as

$$V_{B1} = \frac{1}{4}(W - W_G), \quad V_{B2} = \frac{\pi}{4}(W_M - W_G), \quad (4)$$

where W_G is the work function of free-standing graphene (4.5 eV), W_M is the work function of the contact metal layer (5.4 eV; Ni in this case), and W is the work function of the graphene-covered metal. The parameter β depends on the contact geometry and $\beta = \pi$ when a distance x is large enough compared to d , a thickness of the contact metal ($x \gg d$), where $d \sim 25 \text{ nm}$ in this case. W was evaluated using density functional theory (DFT) calculations⁴³. In the case of graphene on Ni(111), the conical dispersion in the graphene band is destroyed by strong graphene-metal bonding interactions⁴⁴. However, in our process, the resistant residue prevents

chemisorption between graphene and the Ni contact. Later, we can refer the value of an Au contact, which shows physisorption with graphene, and has a work function (~ 5.4 eV) similar to that of a Ni contact. For large graphene-metal separations due to resistant residues, $W-W_G \sim 0.4$ ⁴³. Subsequently, we obtained $\kappa \sim 1.8 \pm 0.9$ for graphene on a hydrophobic substrate and $\kappa \sim 77 \pm 4$ for graphene on a hydrophilic substrate¹ by curve fitting to the measured points in Fig. 7 using eq. (3) with $V_B \sim 0.325$. If we can neglect polarization effects at the graphene channel, the effective dielectric constant κ is given by the average of the dielectric constant of SiO₂ (~ 3.9 eV) and that of the vacuum due to the image effect⁵, i.e., $\kappa \sim 2.5$. This value is close to the experimentally obtained value on the hydrophobic substrate. The large value of κ on the hydrophilic substrate is due to the polarization of the water layer, which has a large dielectric constant at the graphene/substrate interface. Lacking spatial resolution, the interface dipole layer, of the order of several nanometers, cannot be detected in our system. However, the screening potential changes moderately at large values of κ and we can detect spatial shifts in the screening potential by 3D nano-ESCA with a spatial resolution of ~ 100 nm. Therefore, the difference in the potential variation between the hydrophilic and hydrophobic substrates is caused by the difference in the effective dielectric constants, rather than the presence/absence of CTR. Although further theoretical

¹ The estimated value of the effective dielectric constant, κ , is different from our previous study in ref. 22 because we adopted the undoped limit of Eq. (3) as a rough approximation. However, our argument that κ shows larger value on a hydrophilic substrate than typical value of graphene's κ (~ 2.5) is consistent. The chemical potential μ_F , in other words, the doping level of the graphene on the hydrophilic substrate is evaluated compared to the hydrophobic case in this study, so now we can use Eq. (3), which is more general fitting function than a previous study.

investigation with quantum chemistry is required, we believe that the positive charging of graphene due to interactions with a hydrophilic SiO₂ thin film may assist graphene-Ni interactions, which in turn increases the amount of hole-doping in graphene near Ni, assuming that charge transfer occurs through bonding between graphene and Ni in the wide region which is larger than an interfacial dipole layer region.

4. Conclusions

In summary, a combination of 3D nano-ESCA and device characteristics enabled us to quantitatively elucidate that SiO₂ surface chemistry as well as the metal contacts determine the electronic states of graphene channels and consequently, the GFET device performance. By using samples in a device geometry and layer arrangement, we observe a gate voltage induced reversal of the interface dipole orientation. The results obtained will serve as the basis for a quantitative understanding of the GFET operation mechanism, which will help in the realization of high-performance graphene-based devices.

Acknowledgments

This work was supported by the Japan Society for the Promotion of Science (JSPS) through its “Funding Program for World-Leading Innovative R&D on Science and Technology (FIRST Program)” and “Grant-in-Aid for Scientific Research B (Grant Number: 15K17463),” the Ministry of Education, Culture, Sports, Science, and Technology (MEXT) through its “Grant-in-Aid for Scientific Research on Innovative Areas (Grant Number: 26107503),” Japan Science and

Technology Agency (JST) through its “Core Research for Evolutional Science and Technology (CREST),” and “Materials Research by Information Integration” Initiative project and PRESTO (Grant Number: JPMJPR17NB), and the Research Program for CORE lab of “Dynamic Alliance for Open Innovation Bridging Human, Environment and Materials” in “Net-work Joint Research Center for Materials and Devices.” This work was performed at the Synchrotron Radiation Research Organization, University of Tokyo (Proposal Nos. 7402 for 2009–2011, 2012-2014, 2015-2017, and 7435 for 2012).

References

- [1] Geim A, Novoselov K. The rise of graphene, *Nat Mater* 2007;6:183–191.
- [2] Fratini S, Guinea F, Substrate-limited electron dynamics in graphene. *Phys Rev B* 2008;77:195415(1–6).
- [3] Chen JH, Jang C, Xiao S, Ishigami M, Fuhrer MS. Intrinsic and extrinsic performance limits of graphene devices on SiO₂. *Nat Nanotechnol* 2008;3:206–209.
- [4] Nagashio K, Nishimura T, Kita K, Toriumi A. Metal/graphene contact as a performance killer of ultra-high mobility graphene - analysis of intrinsic mobility and contact resistance. *IEEE International Electron Devices Meeting IEDM 2009*. Baltimore, (Maryland. USA), 2009; p.23.2.1–4.
- [5] Ando T. Screening effect and impurity scattering in monolayer graphene. *J Phys Soc Jpn* 2006;75:074716(1–7).
- [6] Nomura K, MacDonald AH. Quantum Hall ferromagnetism in graphene. *Phys Rev Lett* 2006;96:256602(1–7).
- [7] Kotov VN, Uchoa B, Pereira VM, Guinea F, Neto AC. Electron-electron

- interactions in graphene: Current status and perspectives. *Rev Mod Phys* 2012;84:1067–1125.
- [8] Hwang C, Siegel DA, Mo SK, Regan W, Ismach A, Zhang Y, Zettl A, Lanzara A. Fermi velocity engineering in graphene by substrate modification. *Sci Rep* 2012;2:590(1–4).
- [9] Dean CR, Young AF, Meric I, Lee C, Wang L, Sorgenfrei S, Watanabe K, Taniguchi T, Kim P, Shepard KL, Hone J. Boron nitride substrates for high-quality graphene electronics. *Nat Nanotechnol* 2010;5:722–726.
- [10] Ando T, Fowler AB, Stern F. Electronic properties of two-dimensional systems. *Rev Mod Phys* 1982;54:437–672.
- [11] Jang C, Adam S, Williams ED, Sarma SD, Fuhrer MS. Tuning the effective fine structure constant in graphene: Opposing effects of dielectric screening on short- and long-range potential scattering. *Phys Rev Lett* 2008;101:146805(1–4).
- [12] Lafkioti M, Krauss B, Lohmann T, Zschieschang U, Klauk H, Klitzing KV, Smet JH. Graphene on a hydrophobic substrate: Doping reduction and hysteresis suppression under ambient conditions. *Nano Lett* 2010;10:1149–1153.
- [13] Nagashio K, Yamashita T, Nishimura T, Kita K, Toriumi A. Electrical transport properties of graphene on SiO₂ with specific surface structures. *J Appl Phys* 2011;110:024513(1–6).
- [14] Ryu S, Liu L, Berciaud S, Yu YJ, Liu H, Kim P, Flynn GW, Brus LE. Atmospheric oxygen binding and hole doping in deformed graphene on a SiO₂ substrate. *Nano Lett* 2010;10:4944–4951.
- [15] Fukidome H, Kotsugi M, Nagashio K, Sato R, Ohkochi T, Itoh T, Toriumi A, Suemitsu M, Kinoshita T. Orbital-specific tunability of many-body effects in

- bilayer graphene by gate bias and metal contact. *Sci Rep* 2014;4:3713(1–5).
- [16] Lee EJ, Balasubramanian K, Weitz RT, Burghard M, Kern K. Contact and edge effects in graphene devices. *Nat Nanotechnol* 2008;3:486–490.
- [17] Mueller T, Xia F, Freitag M, Tsang J, Avouris P. Role of contacts in graphene transistors: A scanning photocurrent study. *Phys Rev B* 2009;79:245430(1–6).
- [18] Jalilian R, Jauregui LA, Lopez G, Tian J, Roecker C, Yazdanpanah MM, Cohn RW, Jovanovic I, Chen YP. Scanning gate microscopy on graphene: Charge inhomogeneity and extrinsic doping. *Nanotechnology* 2011;22:295705(1–9).
- [19] Horiba K, Nakamura Y, Nagamura N, Toyoda S, Kumigashira H, Oshima M, Amemiya K, Senba Y, Ohashi H. Scanning photoelectron microscope for nanoscale three-dimensional spatial-resolved electron spectroscopy for chemical analysis. *Rev Sci Instrum* 2011;82:113701(1–6).
- [20] Himpsel FJ, McFeely FR, Taleb-Ibrahimi A, Yarmoff JA. Microscopic structure of the SiO₂/Si interface. *Phys Rev B* 1988;38:6084–6096.
- [21] Fukidome H, Nagashio K, Nagamura N, Tashima K, Funakubo K, Horiba K, Suemitsu M, Toriumi A, Oshima M. Pinpoint operando analysis of the electronic states of a graphene transistor using photoelectron nanospectroscopy. *Appl Phys Exp* 2014;7:065101(1–4).
- [22] Nagamura N, Horiba K, Toyoda S, Kurosumi S, Shinohara T, Oshima M, Fukidome H, Nagashio K, Toriumi A. Direct observation of charge transfer region at interfaces in graphene devices. *Appl. Phys. Lett.* 2013;102:241604(1–5).
- [23] Nagashio K, Nishimura T, Kita K, Toriumi A. Mobility variations in mono- and multi-layer graphene film. *Appl. Phys. Express* 2009;2:025003(1-3).
- [24] Yamamoto S, Senba Y, Tanaka T, Ohashi H, Hirono T, Kimura H, Fujisawa M,

- Miyawaki J, Hasarawa A, Seike T, Takahashi S, Nariyama N, Matsushita T, Takeuchi M, Ohata T, Furukawa Y, Takeshita K, Goto S, Harada Y, Shin S, Kitamura H, Kakizaki A, Oshima M, Matsuda I. New soft X-ray beamline BL07LSU at SPring-8. *J Synchrotron Rad* 2014;21:352–365.
- [25] Pirkle A, Chan J, Venugopal A, Hinojos D, Magnuson C. W, McDonnell S, Colombo L, Vogel E. M, Ruoff R. S, Wallace R. M. The effect of chemical residues on the physical and electrical properties of chemical vapor deposited graphene transferred to SiO₂. *Appl. Phys. Lett.* 2011;99:122108(1-3).
- [26] Copuroglu M, Aydogan P, Polat EO, Kocabas C, Süzer S. Gate-tunable photoemission from graphene transistors. *Nano Lett* 2014;14:2837–2842.
- [27] Scardamaglia M, Aleman B, Amati M, Ewels C, Pochet P, Reckinger N, Colomer JF, Skaltsas T, Tagmatarchis N, Snyders R, Gregoratti L, Bittencourt C. Nitrogen implantation of suspended graphene flakes: Annealing effects and selectivity of sp² nitrogen species. *Carbon* 2014;73:371–381.
- [28] Riedi C, Coletti C, Iwasaki T, Zakharov AA, Starke U. Quasi-free-standing epitaxial graphene on SiC obtained by hydrogen intercalation. *Phys Rev Lett* 2009;103:246804(1–4).
- [29] Novoselov KV, Geim AK, Morozov SV, Jiang D, Katnelson MI, Grigorieva I, Dubonos S, Firsov AA. Two-dimensional gas of massless Dirac fermions in graphene. *Nature* 2005;438:197–200.
- [30] Sarma SD, Adam S, Hwang EH, Rossi E. Electronic transport in two-dimensional graphene. *Rev Mod Phys* 2011;83:407–470.
- [31] O'Hare LA, Hynes A, Alexander MR. A methodology for curve-fitting of the XPS Si 2*p* core level from thin siloxane coatings. *Surf Int Anal* 2007;39:926–936.

- [32] Hüfner S. Photoelectron spectroscopy. Berlin Heidelberg: Springer-Verlag;2003.
- [33] Yang CJ, Huang SJ, Kuo CL. The electronic property of graphene adsorbed on the siloxane and silanol surface structures of SiO₂: A theoretical prediction. *Appl Phys Lett* 2012;101:253107(1–5).
- [34] Leung K, Nielsen IM, Criscenti LJ. Elucidating the bimodal acid-base behaviour of the water-silica interface from first principles. *J Am Chem Soc* 2009;131:18358–18365.
- [35] Fukidome H, Pluchery O, Queeney KT, Caudano Y, Raghavachari K, Weldon MK, Chaban EE, Christman SB, Kobayashi H, Chabal YJ. In situ vibrational study of SiO₂/liquid interfaces. *Surf Sci* 2002;502:498–502.
- [36] Wehling TO, Katnelson MI, Lichtenstein AI. Adsorbates on graphene: Impurity states and electron scattering. *Chem Phys Lett* 2009;476:125–134.
- [37] Wehling TO, Lichtenstein AI, Katnelson MI. First-principles studies of water adsorption on graphene: The role of the substrate. *Appl Phys Lett* 2008;93:202110(1–3).
- [38] Newaz AKM, Puzyrev YS, Wang B, Pantelides ST, Bolotin KI. Probing charge scattering mechanisms in suspended graphene by varying its dielectric environment. *Nat Comm* 2012;3:734(1–6).
- [39] Bours L, Guiducci S, M-Kolasińska A, Szafran B, Maan J. C, Heun S. Manipulating quantum Hall edge channels in graphene through scanning gate microscopy. *Phys. Rev. B* 2017;96:195423(1–10).
- [40] Nouchi R, Tanigaki K. Competitive interfacial charge transfer to graphene from the electrode contacts and surface adsorbates. *Appl Phys Lett*

2015;106:083107(1–5).

[41] Giovannetti G, Khomyakov PA, Brocks G, Karpan VV, van den Brink J, Kelly PJ. Doping graphene with metal contacts. *Phys Rev Lett* 2008;101:026803(1–4).

[42] Khomyakov PA, Starikov AA, Brocks G, Kelly PJ. Nonlinear screening of charges induced in graphene by metal contacts. *Phys Rev B* 2010;82:115437(1–6).

[43] Khomyakov PA, Giovannetti G, Rusu PC, Brocks G, van den Brink J, Kelly PJ. First-principles study of the interaction and charge transfer between graphene and metals. *Phys Rev B* 2009;79:195425(1–12).

[44] Dedkov YS, Shikin AM, Adamchuk VK, Molodtsov SL, Laubschat C, Bauer A, Kaindl G, Intercalation of copper underneath a monolayer of graphite on Ni(111). *Phys Rev B* 2001;64:035405(1–6).